THERMAL EXPANSION OF ASYMMETRICAL LAMINATES

Ernest G. Wolff[1]
Associate Professor
Oregon State University

ABSTRACT

Asymmetry in composite laminates originates from materials variability and fabrication errors. This typically enhances bending-extentional coupling. With hygrothermal loading various forms of warping occur. These cause errors in the desired inplane CTE both because of the sample behavior and because of induced errors in the measurement technique. This paper reviews the possible out-of plane strains that may occur during CTE measurements of asymmetrical layups. In addition, measurement techniques and modifications are analyzed which can be used to determine the true inplane strain components. In particular, we address the use of constraints to minimize warping when measuring CTE. Alternatively, one may allow warping but reduce its impact on the measurement by use of compensation optics such as rotating mirror supports or cat's eye retroreflectors. The implications of each approach on CTE accuracy are assessed.

INTRODUCTION

Near-zero coefficient of thermal expansion (CTE) materials have many applications in optics, aerospace, metrology and instrument technology. Extremely low CTE behavior may be found in all major types of materials as well as in engineered structures combining positive and negative CTE's [1]. CTEs of a wide variety of shapes and sizes are of interest, including curved and flat plates, curved/tapered tubes, individual fibers, tows, weaves and cloths, thin films or foils, honeycombs, sandwich panels, coated components, and all types of 1D, 2D or 3D reinforcements. Measured thermal strain values are required in several directions not only as a function of temperature but also as a function of thermomechanical treatment (e.g., thermal cycling), moisture content, applied stress and with possible attachments and/or other constraints. Precise knowledge of CTE levels of 10^{-6}/C or below becomes difficult not only because the thermal strains are small but also because the sample itself may move in ways which mask the true CTE. Analysis of this behavior is required in order to modify measurement techniques to obtain more accurate and reliable CTE data. (Similar considerations hold in the response to changing environmental or hygral conditions, e.g., the coefficient of moisture expansion (CME)).

NONUNIFORM HYGROTHERMAL EXPANSIONS

Intentional asymmetry in composite laminates may be introduced to take advantage of laminate bending-extensional coupling stiffness terms. It may also include interleaving, cladding or coatings. Unintentional asymmetry may arise from fabrication and thermomechanical treatments such in-plane delaminations, the addition of extra plies, incorrect ply sequences, glue lines, materials variability, fabric waviness or wrinkles, tow misalignment, asymmetry in molding systems, and manufacturing errors such as high pressures with direct tow-tow contact [2] or ply slippage before gelation [3]. Non-uniform resin extraction, variations in ply thicknesses, and global variations in braid angles may also result in asymmetrical layups. When parts have a double curvature, forming may result in out-of-plane shear deformation and rearrangements of fibers [4]. Unsymmetrical residual stresses caused by nonuniform cooling and/or asymmetrical layups will develop from elevated fabrication temperatures. Microcracking developed during hygrothermal cycling, e.g., too low temperatures may also exaggerate the effects of other asymmetries [5]. Edge/end effects may in principle cause warping, e.g., in a non-circular sample because

---

[1]Department of Mechanical Engineering, Oregon Sate University, Corvallis, OR 97331

the orthotropic construction is modified by non-orthotropic stress states. Non-uniform moisture gradients during hygral equilibration may cause warping [6].

ANALYSIS

A) Laminate Theory

While classical laminate plate theory (CLPT) does not always predict the correct deformations [7,8], its equations provide a necessary initial relation between (midplane) strains and applied stresses and moments:

$$\left[\frac{\{e^o\}}{\{k\}}\right] = \left[\frac{A' \mid B'}{B' \mid D'}\right]\left[\frac{[N]}{[M]}\right] \tag{1}$$

where $\{e^o\}$, $\{k\}$ are the mid-plane plate strains and curvatures. N, M, are the total mechanical (M), thermal (T) or hygral (H) stress and moment resultants, respectively. Thus

$$\begin{aligned} [N] &= [N^M] + [N^T] + [N^H] \\ [M] &= [M^M] + [M^T] + [M^H] \end{aligned} \tag{2}$$

where

$$N^T,\ M^T = \int [Q']_k \{a\}_k \Delta T,\ z,\ dz \tag{3}$$

A', B', and D' are the completely inverted stiffness [A], coupling [B] and flexural or bending [D] stiffness matrices. The off-axis laminae stiffnesses Q'_{ij} depend on ply stiffnesses and Poisson's ratios. The B_{ij} components imply coupling between extension and bending or twisting of a laminate;

$$[B'] = -[A^{-1}][B]\left([D] - [B][A^{-1}][B]\right)^{-1}, \tag{4}$$

Note that if $[B] = 0$, $[B'] = 0$. In general, it is desired to know the axial, in-plane coefficients of thermal expansion, a^{oT};

$$\begin{bmatrix} e_x^{oT} \\ e_y^{oT} \\ \gamma_{xy}^{oT} \end{bmatrix} = \begin{bmatrix} \alpha_x^{oT} \\ \alpha_y^{oT} \\ \alpha_{xy}^{oT} \end{bmatrix} \Delta T \tag{5}$$

Thus from Equations 1 and 5, assuming zero mechanical or hygral stress or moment resultants,

$$\alpha_x(\Delta T) = e_x^o = A'_{11} N_x^T + A'_{12} N_y^T + A'_{16} N_{xy}^T + B'_{11} M_x^T + B'_{12} M_y^T + B'_{16} M_{xy}^T \tag{6}$$

We note that the $[A']$, $[B']$ and $[Q']$ as well as the ply properties, $\{a\}_k$ in Equation 3 are temperature dependent [6]. The total strains are given by

$$\{e\} = \{e^o\} + z\{k\} \tag{7}$$

where z is the distance from the laminate midplane. This indicates that if the curvatures $\{k\}$ are zero, that the total in-plane strains will correspond to the desired midplane strains $\{e^o\}$.

B) Warping of Asymmetrical Laminates

CLPT was used to calculate the curvatures (k) resulting from uniform hygrothermal loads for different classes of laminations. In general, whenever the [B] matrix terms were all zero, the curvatures from a ΔT load were also zero. For a flat laminate, this means the ply layup must be symmetrical about the midplane to avoid out-of-plane distortions. Antisymmetric layups have zero [B] terms except for B_{16} and B_{26} and this generally leads to a twist on thermal loads. A curved panel will still be subject to this twist. A class of layups reported by Winkler [9] is an exception – even though the [B] matrix terms are non-zero, one can still find an absence of out-of-plane curvatures on hygrothermal loading. Thermal deformations of anti-symmetric laminates at cure were examined by Fukuda and co-workers [8] who found that deformation differed from that predicted by CLPT, and some improvement with a theory based on energy principles was obtained. Table I summarizes the expected curvatures.

Table I. Curvatures [k] as a Function of [B] Matrices

Type of Laminate	[B]	[k]
Symmetric Flat	0	0
Asymmetric Flat	≠0	≠0
Antisymmetric Flat	≠0	≠0
Asymmetric Flat (HTCC)*	≠0	0
Symmetric Curved	0	≠0
Antisymmetric Curved	≠0	≠0
Asymmetric Curved	≠0	0 = possible

*Hygrothermally Curvature Stable Coupling [9], e.g.,
$[\theta^1,(\theta^1 + 90)_2, \theta^1, \theta^2, (\theta^2 + 90)_2, \theta^2]_T$ where $\theta^1 \neq \theta^2$

As a numerical example, we consider a symmetrical quasi-isotropic 8-ply laminate of T300/5208 graphite epoxy $[0/+45/-45/90]_s$. The B_{ij} terms are essentially zero and a 100°C excursion will lead to a midplane strain of 152 μe, with no curvature or twist. If the ± 45 plies on one side are interchanged in position, we have significant B_{16} and B_{26} terms, a twist of $k_6 = 0.35\ m^{-1}$ and a predicted midplane strain change to 157 μe. Then twist may easily mask the strain change unless it is restrained.

C) Use of Constraints for CTE Measurement

Assume a plate is initially bowed so that the center sits a distance d above the ends. Consider a minimum distributed load (q kg/m) to impose a negative axial moment resultant and hence flatten the sample. (Distributed loads are preferable to concentrated loads for both mechanical and thermal uniformity.) Then

$$d = (5\ q\ L^4)/(384\ E_f\ I) \tag{8}$$

where

$$I = b\ h^3/12 \tag{9}$$

I is the moment of inertia and E_f is the flexural stiffness (kg/cm^2), dependent on the ply layup. The corresponding moment (applied at both ends) caused by this weight is

$$M = M_1 * b = q\,L^2/8 \tag{10}$$

where M_1 is the moment per unit width. The curvature [10] is

$$k_1 = M/E\,I = C\,d/L^2 \tag{11}$$

where C is a numerical constant. As an example, assume a plate 15.2 × 1.27 × 0.1 cm (with 8 plies each 0.0127 cm thick) for a CTE measured in the 15.2 cm direction and d = 0.25 cm. If the layup is $[0/+45/-45/90]_s$ of T300/5208 graphite/epoxy, $E_f = 1.19\ e^6$ kg/cm^2 (16.9 e^6 psi). Table II summarizes the calculations.

Table II. Summary of Restraint parameters for Example

	Symbol	Units	Distributed Load	Concentrated Load
Total Load	P	(kg)	0.689	0.430
Moment Resultant	M_1	(kg)	1.03	1.28
		(MN)	10.1 e^{-6}	12.6 e^{-6}
Constant Eq. 9	C	—	9.6	12
Curvature	k_1	(cm^{-1})	0.010	0.013
		(m^{-1})	1.0	1.3

Hence a 0.689 kg load at the center or a -1 kg moment resultant applied at both ends will exactly flatten this laminate. Laminate theory indicates that there is a zero effect on e^0 as a result of this restraint, but that is because the [B] terms for this layup from Equation 4 are zero.

The corollary to obtaining bending/twist or curvatures when a hygrothermal (or mechanical) extensional force is applied is that a laminate with non-zero B_{ij} terms can not be subjected to moments without at the same time suffering extension of the middle surface. Any layup with non-zero [B] terms will exhibit substantial midplane extensional microstrains when subjected to a moment even as small as that used to flatten the 8-ply laminate of the example above. If the restraint used is a dead weight distributed load, that is, M_1 = constant, $M_2 = M_6 = 0$, the initial in-plane strain will remain constant and not present an error, as only changes in strain are of interest to thermal expansion measurements. However, if the restraint is attempted on laminates with non-zero [B] terms with loads that may change during temperature changes in the restraint system, significant errors may result. Similarly, from Equation 4, if the [B] coupling terms change during the thermal excursion under restraint, errors in e^0 measurement will result. Since

$$B_{ij}(T) = \frac{1}{2} \sum \left(Q'_{ij}(T)\right)\left(h_k^2 - h_{k-1}^2\right) \tag{12}$$

The initial response should be to keep restraints small so that the [B(T)] terms will have minimal effect.

D) Effect of Stress on the CTE

Internal stress relief, such as microcracking, will change the ply stiffnesses and hence the laminate terms [A′], [B′] and [D′]. The change in CTE with stress or thermal cycling is of frequent interest. Clearly, changes in the coupling stiffnesses with temperature complicate the errors from restraints. If microcracking occurs, the result may be to create or enhance the [B] terms unless both the layup and the microcracking are symmetrical. Again, if the effect of in-plane stresses [N] on the CTE are of interest, any non-zero [B] terms will generate moments or

warping. The applied in-plane stress (e.g., N_1) tends to provide some restraint, but errors arise if moments M_2 or M_6 are induced.

To determine if a weight may cause ply microcracking due to the resultant stresses, we again take T300/5208 with the quasi-isotropic layup and a 0.9 kg applied M_1. The maximum stresses occur in the outer plies to a maximum level of about 1.24 MPa. This gives a first ply failure safety margin, R-value [10], of about 32. We conclude, therefore, that adding a weight to flatten a curved or twisted sample has a negligible effect on the measured CTE.

RESULTS

The effects of sample bend/twist are shown in Figure 1 for a 4.0 x 18.0 x 0.01 cm graphite fiber/resin composite specimen which was measured horizontally in the 18 cm direction three times. (The interferometry technique used is described later.) On the first two measurements there was no weight placed on the sample to keep it flat. One side faced up during the first measurement; the other during the second. With side #1 facing up, the total strain was 600 ppm greater than with side #1 facing down, giving CTEs of -0.71 ppm/C and -0.99 ppm/C, respectively. When 50 grams of mass was uniformly placed on side #1 the prior concave bending was eliminated and the CTE was correctly measured as -0.88 ppm/C, near the average of the other two measurements. (The variation in these three measurements is far greater than the repeatability and accuracy of these values (0.01 ppm/C).)

EXPERIMENTAL

A) General Techniques

CTE measurements of laminates are made by LVDT based dilatometers, and interferometers such as Michelson, Fizeau, Fabry-Perot, speckle, and shearography. Optical levers, capacitance, Moire, strain gages and other methods also have problems with warping samples. Adoption of distortion insensitive CTE measurement techniques is difficult because most linear displacement devices can not differentiate between e^o and e. Auto-collimators may be added to any linear measurement techniques to determine plate sample bowing or curvatures, changes in parallelism of tube faces and/or tube axis bending, twists, and other distortions. They need to be coupled with simultaneous total axial strain measurement.

Here the bowing error for linear dilatometers and for Michelson interferometers is analyzed. It is shown that fringe analysis of an interferometer can be used to correct for bowing. Finally, several means for maintaining the fringe pattern are outlined, even though the sample is warping.

B) Corrections for Sample Bowing in a Dilatometer

The displacement direction is assumed to remain aligned with the original sample axis. Suppose a plate is loosely supported vertically and a vertical thin (quartz) rod rests on the midplane. Assume the CTE is exactly zero but that circular curvature or bowing develops. The error in displacement due to the bowing is given by

$$\Delta = L_o - L_{eff} = L_o - 2R \sin\left(L_o/2R\right) \tag{13}$$

where L_o is the original length, L_{eff} is the perceived length due to bowing and $L_o/2R$ is in radians. For example, if L_o = 5 cm, and R = 25 cm, the error is 1666 microstrain, whereas if R = 250 cm (smaller k_1) the error is only 16.7 μe. This equation can be expressed in terms of the curvatures by substituting $k_1 = 1/R$. Thus if the sample is separately measured or predicted (with CLPT) to show a curvature $k_1 = 1\ m^{-1}$, the total measurement error will be 104 μe.

C) Corrections for Michelson Interferometer

Michelson interferometry is taken as a case study because of its versatility in the contactless CTE measurement of a wide variety of sample shapes and sizes. Figure 2 illustrates the basic optical system used to measure the inplane CTE of a plate sample. Laser beams are typically reflected off mirrors mounted on sample ends or faces, or the sample itself is used as a reflector. The returned beams must overlap at the sp beam splitter (as well as the initial beam splitter) for a fringe pattern to be analyzed. Figure 3 shows a typical trace of the fringe pattern change when a sample is cooled from about 6 deg to -12 deg and reheated to almost 5 deg. The voltage traces of the two detectors after the sp beam splitter show an expansion direction change when the temperature changes. There is a slight decrease in detector amplitude on initial cooling but basically this sample does not warp on cooling/heating. With no warping, the change in optical path length difference of the two interferometer arms (fringe motion) relates directly to the midplane strain e^o.

Bending causes reflected beam divergence which in turn causes reduced photodetector signals and extra fringe counts. Figure 4 shows a significant amplitude change as the sample is heated from about -40 to 70 deg. Bowing causes the reflected beams to move apart after being initially superimposed on the beam splitter. To analyze the effect of bowing in the vertical plane we take the case that the beam splitter is also in a vertical plane. Then the reflected beams (of diameter d_B) diverge until their overlap is minimal. The signal is greatly reduced if the total vertical reflected beam deflection equals the beam diameter. In geometrical terms (Figure 5), and ignoring the slight axial displacement of the mirrors, the rear mirror beam moves up; the front reflection moves down until

$$(a + b + L_o) \sin \theta + a \sin \theta = d_B \tag{14}$$

The corresponding sample bowing or curvature is obtained from

$$k_1 = \theta \text{ (radians)} / L_o \tag{15}$$

This defines the maximum curvature of the sample before the signal is lost. (Figure 5 is conservative; the beams must still coincide to some extent at the detector as well at the beam splitter.) Appendix A derives the measured strain error corresponding to this curvature.

$$\Delta OPLD = \frac{a + d + b + L_o - \Delta}{\cos \theta} - \frac{a - d}{\cos \theta} + 2d - b - L_o - \Delta \tag{16}$$

if y is the perpendicular from the midplane to original mirror line,

$$d = (z - y) \sin (\theta/2) \qquad \text{where } z < y < 0 \tag{17}$$

Then d increases from zero to z as k decreases from infinity, depending on where the mirrors are relative to the sample ends. Dividing Equation 14 by L_o gives the bowing strain error or correction to the true midplane strain e^o. Equation 14 defines θ. As a numerical example, suppose $L_o = 0.05$ m, a = 1 m, b= 0.02 m, z = 0.005 and $d_B = 0.003$ m. Then from Equation 14, θ is 1.45 e^{-3} radians. From Equation 15, k_1 max is then 0.029 m^{-1}. Inserting this value into Equation 11 gives $\Delta = 4.38\ e^{-9}$ m. Equation 17 predicts $d_{max} = 3.625\ e^{-6}$ m (if y = 0). Equation 16 then predicts a change in OPLD of 1.45 e^{-5} m or a 290 μe error.

It is useful to note that the biggest terms here are due to the separation of the midplane from the beam reflection point (z). Indeed d far exceeds Δ in this example. As z approaches zero, d also goes to zero and the residual error (at k_{max}) is 9.8 e^{-8} m or 1.92 microstrain. The error can be quantified directly from the fringe amplitude changes. Basically, the error is proportional to the overlap area of the two reflected beams. (This correction can be built into an automatic fringe analysis system.) If the angle the two non-diverging Gaussian beams are misaligned is $\theta/2$ (Figure 5), then the loss factor is given by Rowley [11] as

$$F = \exp\left\{-\left(\pi\, d_B^2\, (\theta/2)\right)^2 / \left[\lambda^2 \left(2\, d_B^2\right)\right]\right\} \tag{18}$$

For λ = 632.8 nm and d_B = 1 mm , F = 0 as expected for the warping situation above which gave loss of signal. With $\theta/2 = 1\ e^{-4}$ radians, the signal is reduced to 76% of the original amplitude.

If the sample twists rather than bows, the return beams are displaced out of vertical plane. This adds an additional apparent strain because one or both of the return beams are displaced 45°, the horizontal beam splitter orientation relative to input beams. This gives strain error up to $(d_B)\sin 45°$. Increasing the B/S - detector distance will reduce this error because the AC signal will be lost. Careful observation of return beam orientations is needed to make adequate corrections and/or to characterize the twist.

D) Warping Insensitive Methods

It has been shown that flat mirrors mounted in a fixed manner on samples will provide reflections which are sensitive to rotations caused by sample warping. There are instances, however, when samples warp in several directions simultaneously, or when the bowing can be separately monitored, or when the sample does not bow but the support system causes rotations which may result in signal loss. Warping may also be considered negligible compared to the overall thermal (or hygral) strain and continuous measurements over the entire hygrothermal range are desired. In these instances, it is desirable to maintain the detector signals continuously in spite of the warping, and be subject primarily only to the dilatometer error outlined in section B.

Figures 6 and 7 show two modifications to the fixed mirror mounting which minimize the signal effects of sample warping. The pin method involves mirrors sliding on a fixed (low expansion material) track. A disadvantage is the spacing needed for pin/hole clearance; on direction changes there is a lag. The blade method used for the data of Figure 1 and shown in Figure 7, employs shallow, 0.3 mm wide grooves inscribed on the sample perpendicular to the measurement direction. Reflecting steel razor blades are connected to quartz rods. ULE mirrors may also be attached to the blades, which are free to rotate to maintain perpendicularity to the laser beams. The length of the support rods can be adjusted to minimize the response of the mirrors to warping. This system also assures that there is instantaneous response to direction changes.

E) Retroreflector Technology

Retroreflectors are passive optical systems that return incident light at an angle of reflection exactly opposite the angle of incidence. Since the optical measuring system is not sensitive to sample warping (the angle of beam incidence remains fixed), a retroreflector is a prime candidate for offsetting (fixed) reflector rotations. A familiar type, the corner cube, is often mounted on machine tools or parts for use with interferometric alignment systems. Solid corner cubes can not be used reliably for thermal expansion measurements, however, because their internal optical path lengths can not be predicted or controlled as a function of temperature, since both the expansion of the material and its index of refraction will vary with (unknown) temperature gradients. Open corner cubes have been used, at least to cryogenic temperatures [12]. Problems for general use, however, include size and cost, internal and mounting stresses, thermal gradients and a need for three optical elements or surfaces.

A more promising approach for thermal expansion is the use of catadioptic afocal lenses, or cat's eye retro-reflectors [13-15]. This approach uses two optical elements; a concave mirror (which may be planar, spherical, or parabolic) mounted on the sample and either a thin double convex lens or a secondary reflector, mounted at the focal point distance in front of the mirror. The latter can be shielded from the sample's temperature excursions. In principle, rotations of the sample mirror will still allow maintenance of exactly a 180° reflection angle.

A brief error analysis of the preferred type of cat's eye reflector is based on Figure 8 [15]. The two main errors are due to displacement and tilt of the secondary mirror from the focus position. The total angular error is given as

$$\Delta r_o' \Big|_{d=f} = \left[(2\alpha/f) + \left(2r_i/f^2\right) + 2r_i'(1/R - 1/f)\right] \Delta d \qquad (19)$$

where r_i is the (radial) input ray height, and r_1', r_o' are the slopes of the input and output rays, respectively. f is the focal length of the lens, d the lens mirror distance and α, R the tilt and radius of curvature of the reflecting secondary mirror. When d = f, r_o' equals r_1', a true cat's eye reflector. The system is optimum if R = f but a

plane mirror has R = ∞. Typically, $\Delta d = 10^{-5}$ m from thermal expansion. If f = 0.1 m, $r_i = 5 \times 10^{-4}$ m, $r_i' = 0$, and $\alpha = \theta/2 = 1e^{-4}$ radians, then $\Delta r_o' = 1\ e^{-6}$ radians. As the CTE decreases, Δd and hence $\Delta r_o'$ decrease and the error due to sample warping (tilt) or α goes to zero. Also note that if $\theta = \alpha = 0$, a finite Δd imposes no error.

Since they are part of the optical path lengths of the interferometer [16], errors will also arise if the temperatures of the lenses used change differently from one another; their temperature or its distribution do not need control otherwise. Thus use of cat's eye reflectors allows continuous measurement of the in-plane CTE without signal loss. The only practical drawback is that their use means extra optical components and reflected beams go back into the laser. Standard half wave plates with polarizers or Faraday isolators provide >3 dB isolation.

DISCUSSION

Low stiffness structures present special measurement problems. Thin films or foils, fibers, tows, yarns, unreinforced fabrics and honeycomb structures without face sheets are typical examples. In-plane CTE of thin films are readily measured with Michelson interferometry if they can be treated as low stiffness thin plates, viz., by adding weights. Honeycombs can be measured along the cell directions (material direction) in the same way. Problems arise with short length thin films or with directions across the cells in a honeycomb. In these cases alternative methods to Michelson interferometry must be considered. Speckle interferometry is a good candidate for inplane film or fiber CTE, holographic interferometry or machine vision systems [17] may be considered for 3-D deformation of a honeycomb structure. However, resolution, complexity (and cost) may be drawbacks. Elimination of warping, e.g., due to ply misorientations, is likely to require unique combinations of improved design and fabrication [18].

CONCLUSIONS

Sources of non-uniform expansions (or contractions) in laminated materials have been reviewed. Sample asymmetry can lead to significant errors in CTE measurement because of the extension-bending or twisting coupling, expressed by non-zero [B] stiffnesses in the laminate theory. Thus, efforts to mitigate warping to allow continuous CTE measurement may influence the CTE results obtained.

We have addressed warping of test samples from the viewpoints of prevention and correction of warping, and discussed schemes for making the CTE measurement system insensitive to warping. Restraints are feasible and may not present errors unless the stresses and moments employed change with temperature.

Sample bowing can be monitored by an optical lever system; the angle of interferometer return beam divergence relates to the curvature variation with temperature. Photodetector signals record AC signals (fringe motion) which give in-plane strain; while the amplitude (DC level) records beam divergence caused by plate bowing. Correction of in-plane derived strain from changing amplitudes is complex as precise geometry of the optics must be taken into account.

In certain instances, warping may be ignored from the CTE data viewpoint but may still present measurement problems. Methods which decrease sensitivity to warping include use of pin connections, rotating blade mirrors and retroreflectors such as cat's eye systems.

Finally, the total hygrothermal strain response of the sample or structure may be of interest. In this case, holographic, speckle or Moire interferometry or machine vision systems have specialized applicability.

ACKNOWLEDGMENTS

The author gratefully acknowledges the assistance of the staff of Precision Measurements and Instruments, Inc., P.O. Box 34, Philomath, OR 97370, for the material presented in the figures and for helpful comments based on their analysis of considerable CTE data.

REFERENCES

[1] E.G. Wolff, *Thermal Expansion - 8*, Ed. T.A. Hahn, Plenum, 211 (1984).

[2] J. Chen, Proc. ICCM-10, Whistler, B.C. Canada, III-221 (1995).

[3] J. Shi and R. Flannigan, Proc. ICCM-10, Whistler, B.C., Canada, III-197 (1995).

[4] T. Vu-Khanh and B. Liu, *Comp. Sci. & Tech.* **53**: 183 (1995).

[5] E. Adolfsson and P. Gudmundson, *Comp. Engrg.* **5**: 107 (1995).

[6] E.G. Wolff, Proc. ICCM-8, S-I, SAMPE, July (1991).

[7] K.J. Yoon, P.J. Kim, T.W. Kim and E.J. Jun, Proc. 40th Intl. SAMPE Symp., 1026 May (1995).

[8] H. Fukuda, K.Takahashi and S. Toda, Proc. ICCM-10, Whistler, B.C., Canada, III-141, (1995).

[9] S.J. Winkler and S.C. Hill, Proc. ICCM-8, SAMPE, 2-I, (1991).

[10] S.W. Tsai, *Composites Design,* 4th ed., Think Composites Inc., 9-2, (1988).

[11] W.R.C. Rowley, National Physical Laboratory, (U>K>), Report MOM78, (1986).

[12] R. Hofmann, R. Katterloher and P. Essenwanger, *Appl Optics* **25**: 4614 (1986).

[13] R.F. Chang, D.G. Currie and C.O. Alley, *J. Opt. Soc. Am.* **61**: 431 (1971).

[14] R. Beer and D. Marjaniemi, *Appl. Optics* **5**: 1191 (1966).

[15] J.J. Snyder, *Appl. Optics* **14**: 1825 (1975), also **15**: 1691 (1976).

[16] E.G. Wolff and S.A. Eselun, *Rev. Sci. Instr.* **50**: 502 (1979).

[17] M. Norris, D. Oakes and E.G. Wolff, Proc. 40th Intl. SAMPE Symp., 1855 May (1995).

[18] D. Rapp, M.C. Lou and C.-P. Kuo, NASA Tech. Briefs, 68 March (1995).

APPENDIX A - Derivation of Equation 14

As Figure 5 indicates, the rear mirror will reflect at $+\theta$, the front mirror by $-\theta$. The rear mirror distance to the beam splitter increases from $a+b+L_o$ to $(a+b+L_o)/\cos\theta$, while the front beam path increases from a to $a/\cos\theta$. At the same time, the rear mirror moves towards the beam splitter, by virtue of the Equation 13 effect. Similarly, the front mirror moves away from the beam splitter giving an apparent sample length decrease.

A) Final OPL to rear mirror $= \left(a - d + b + 2d + L_o - \Delta\right) + \dfrac{a - d + b + 2d + L_o - \Delta}{\cos\theta}$

B) Front mirror final OPL $= (a - d) + (a-d)/\cos\theta$

C) Front mirror initial OPL $= 2(a + b + L_o)$

D) Front mirror initial OPL $= 2a$

E) Initial OPL difference (OPLD) = (C - D)

F) Final OPLD = (A - B)

G) Total change in OPLD = ΔOPLD = (A-B) - (C-D) = Equation 16

Figure Captions

1) Thermal expansion of unidirectional graphite/resin panel (from [17]).

2) Horizontal laser interferometer.

3) Interferometer photodetector signals and temperature trace of a cooled/heated sample showing direction change without warping.

4) Photodetector signals and temperature trace from a Michelson interferometer with a warping sample.

5) Analysis of a bowing sample showing divergence of reflected laser beams from fixed mirrors.

6) Pin system for CTE measurement from a (possibly) warping sample.

7) Blade system for decreasing sensitivity to sample warping in a Michelson Interferometer CTE measurement system.

8) Parameters of a Cat's eye retroreflector (from [15]).

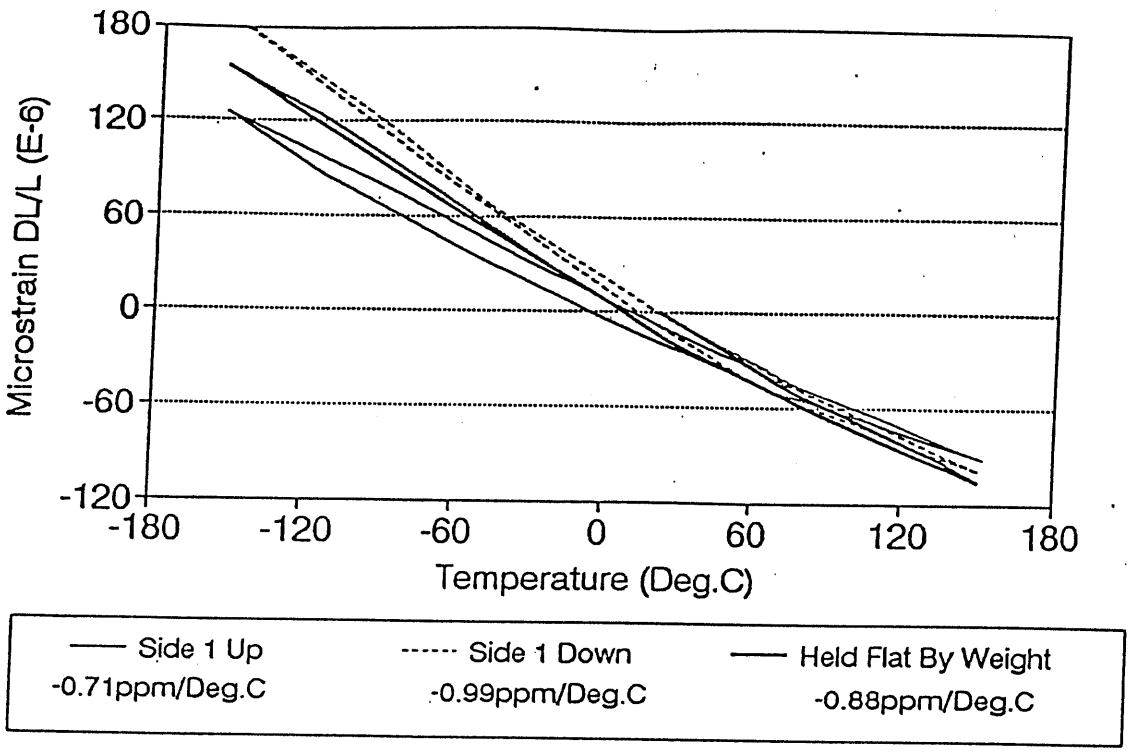

Figure 1 Thermal Expansion of Unidirectional Graphite/Resin Panel [17]

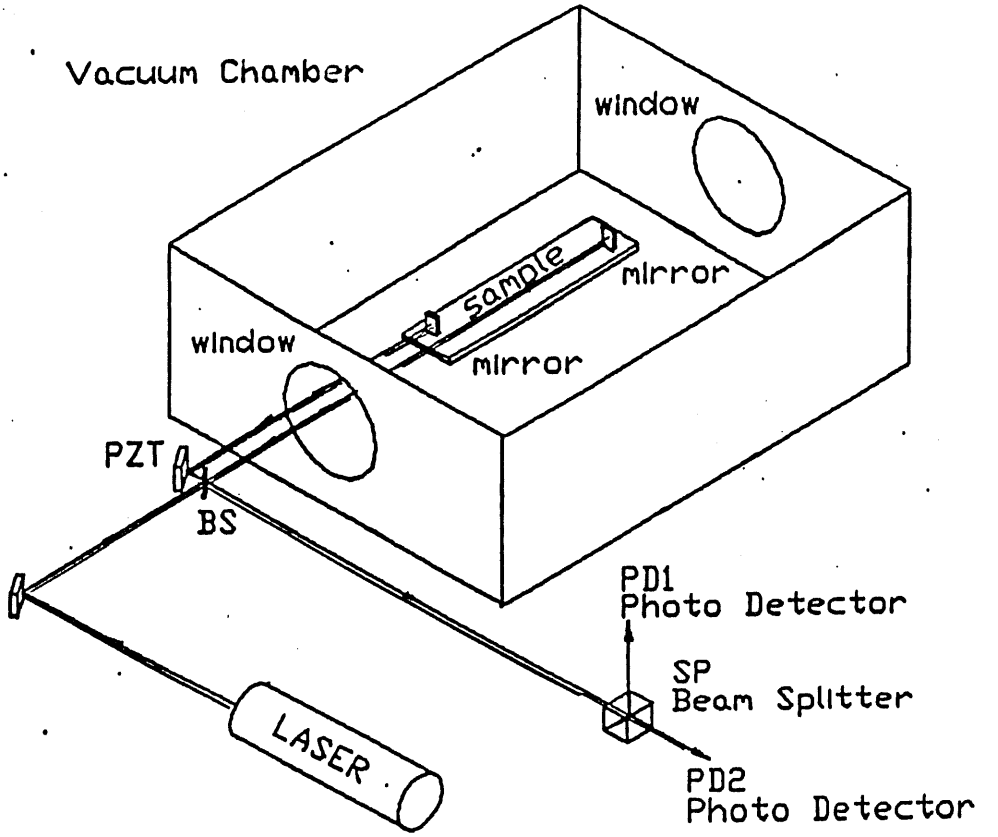

Figure 2. Horizontal LASER Interferometer

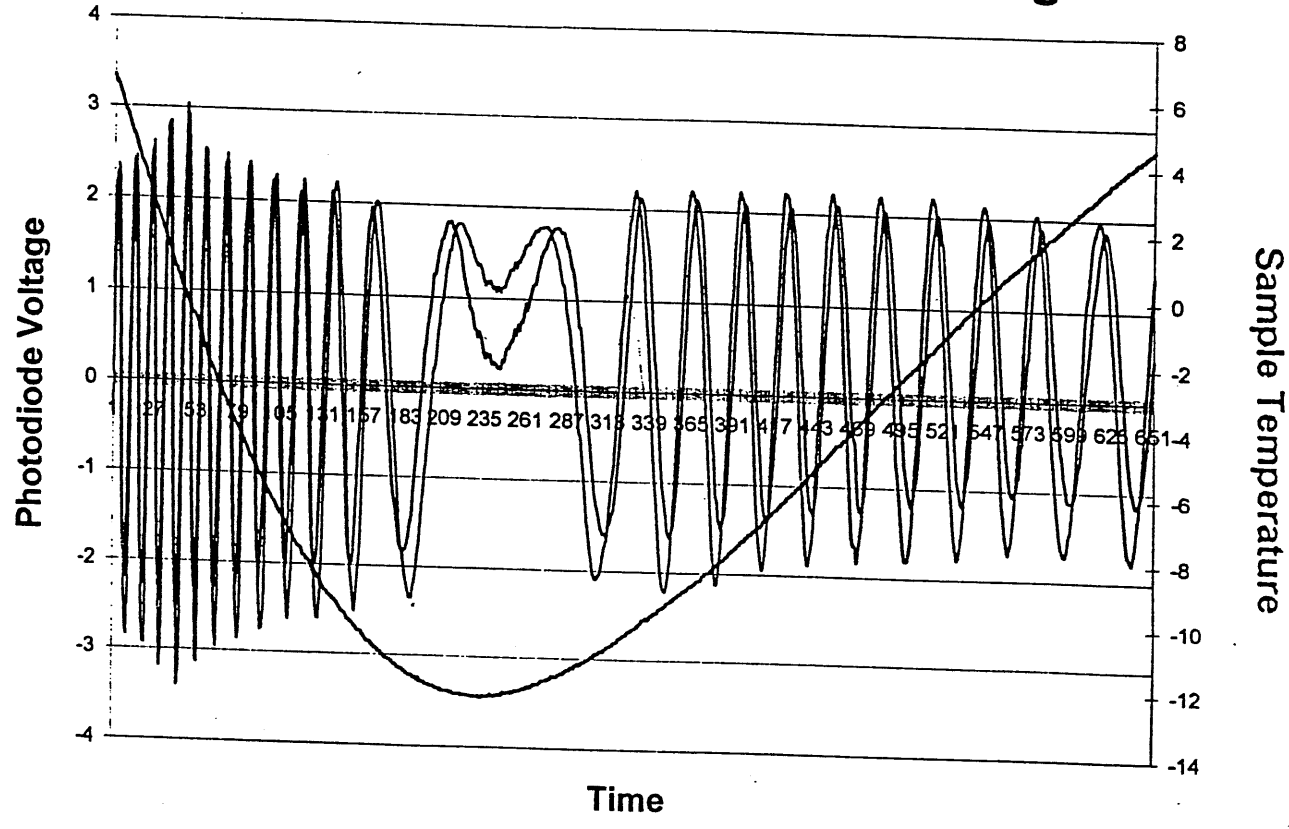
Example of Direction Change
Photodiode Voltage
Sample Temperature
Time
4
3
2
1
0
-1
-2
-3
-4
8
6
4
2
0
-2
-4
-6
-8
-10
-12
-14

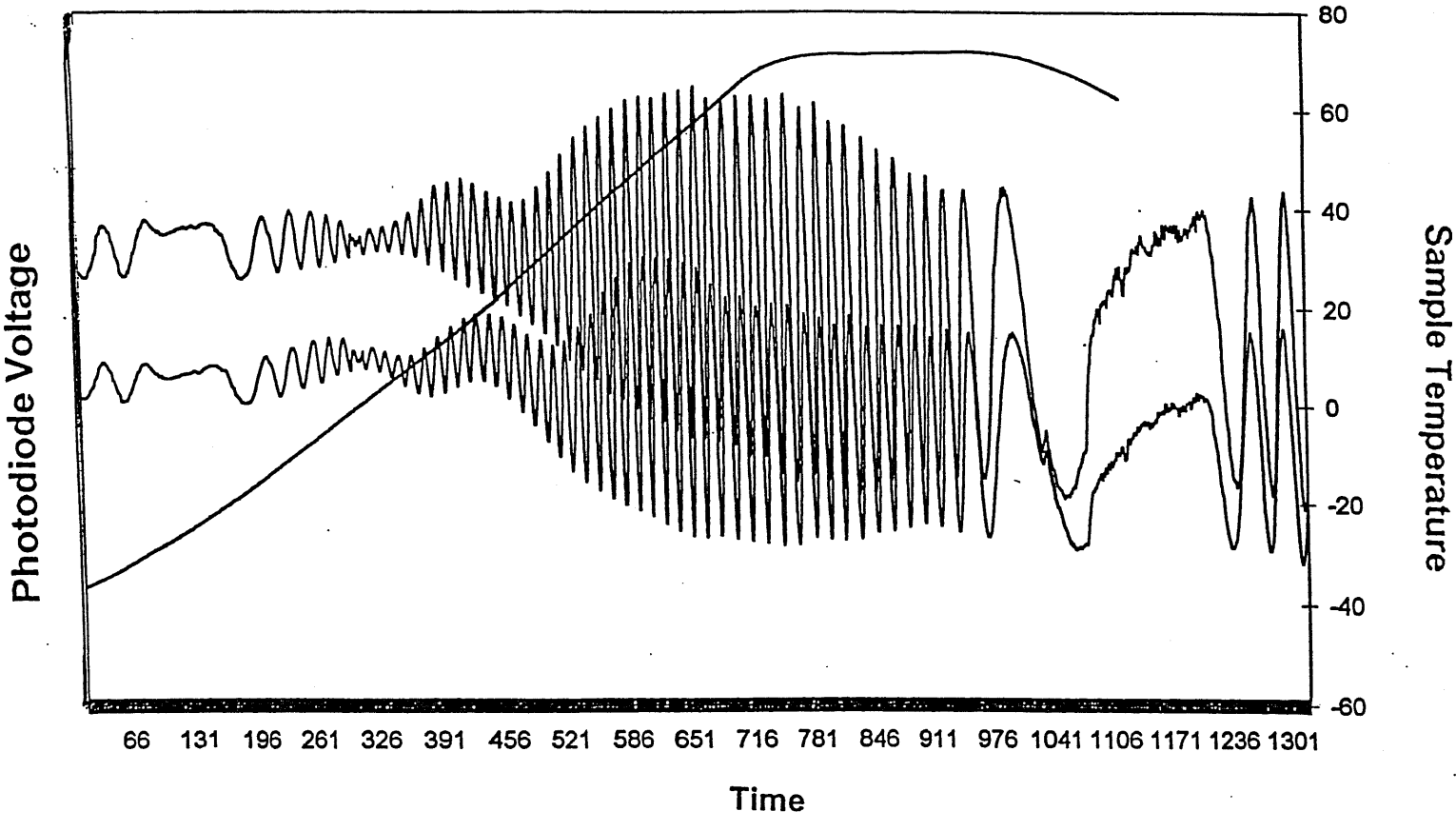
Photodiode Voltage
Sample Temperature
80
60
40
20
0
-20
-40
-60
66 131 196 261 326 391 456 521 586 651 716 781 846 911 976 1041 1106 1171 1236 1301
Time

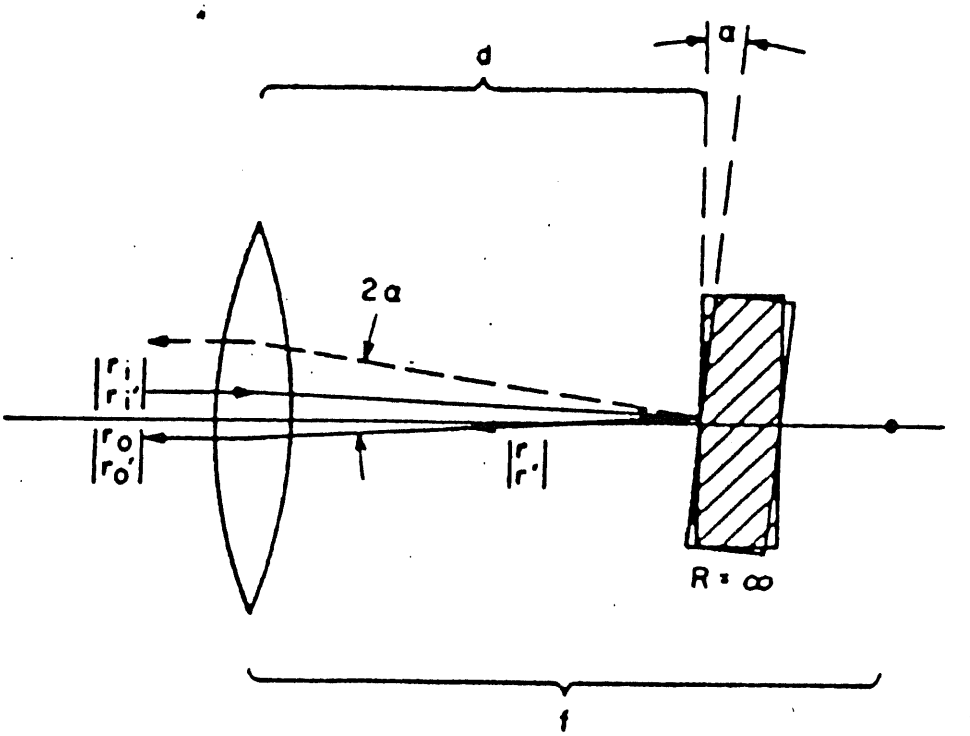
d
a
2α
R = ∞
f

Fig. 6 Pin System

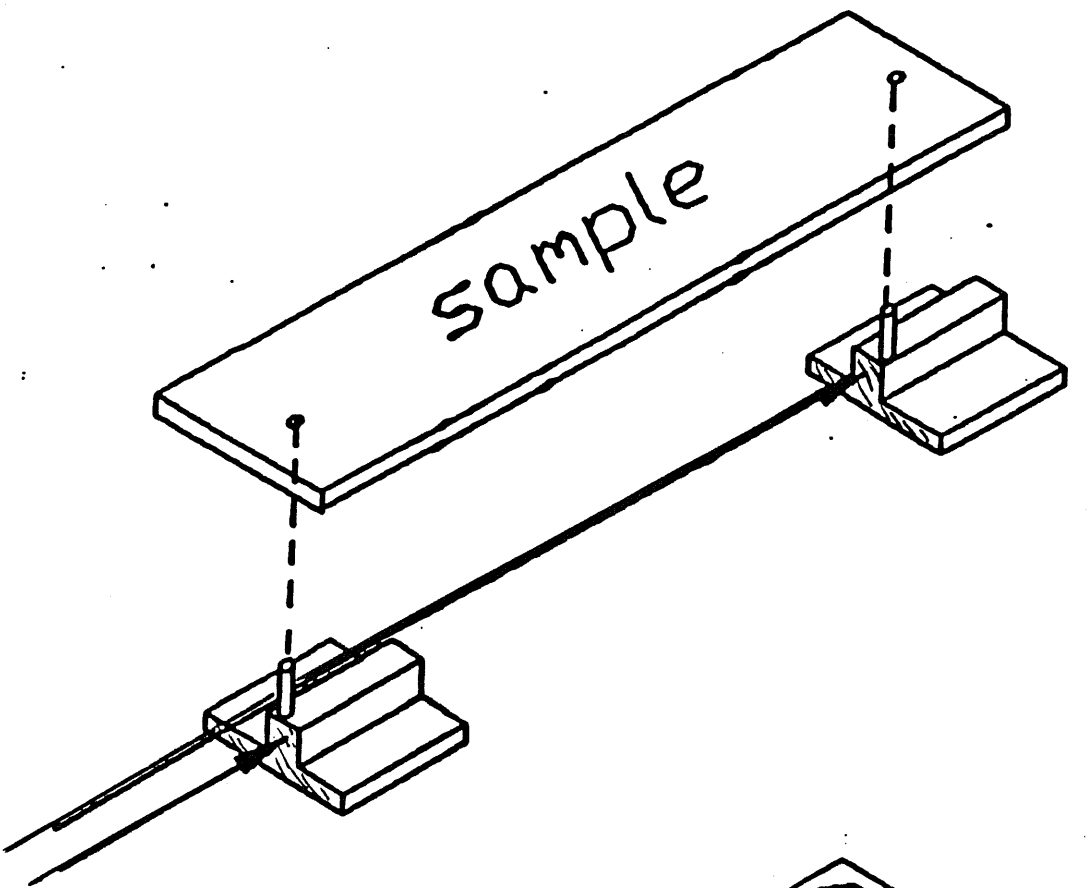

Fig. 7 Blade System

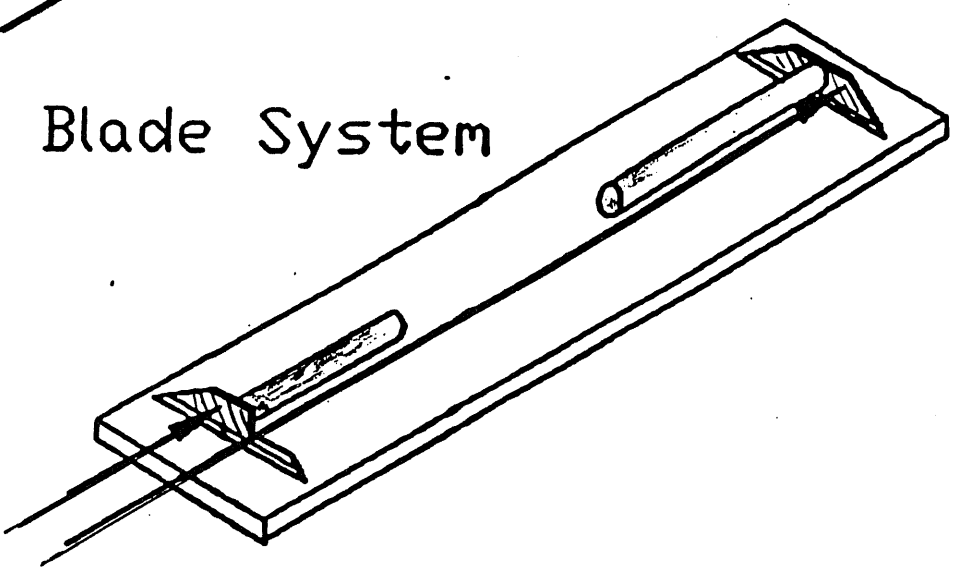

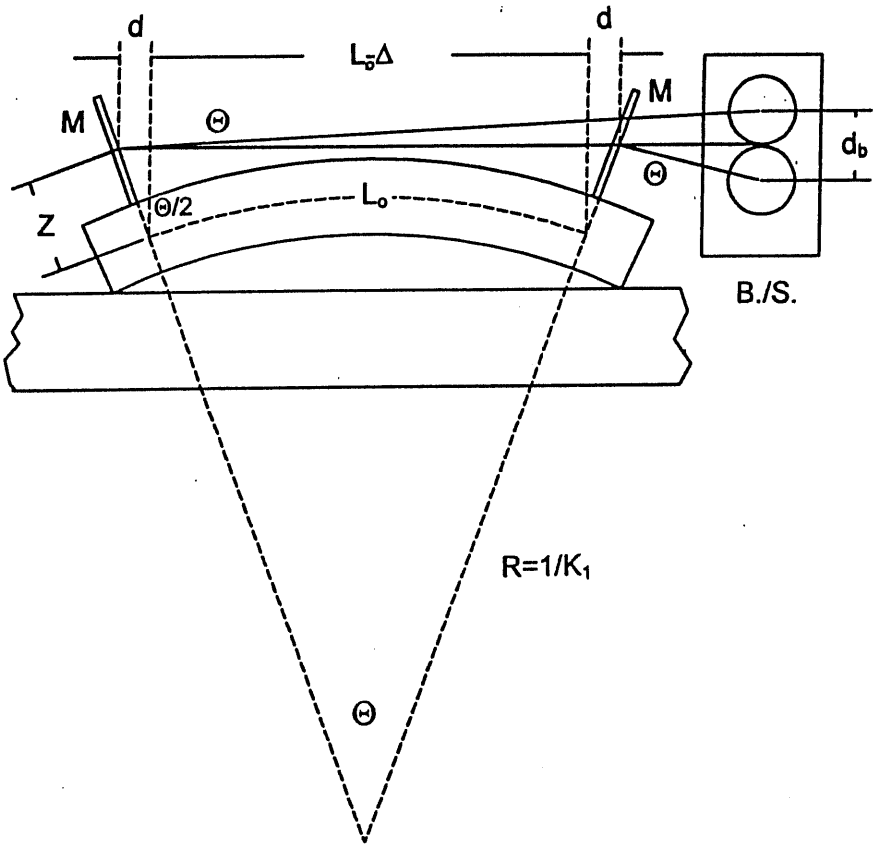
d
$L_o \pm \Delta$
d
M
M
Θ
Θ
d_b
Θ/2
L_o
Z
B./S.
$R=1/K_1$
Θ